Original Article

Pan-cancer prognostic model and immune microenvironment analysis of natural killer cell-related genes

Caihong Li[1#], Yuxin Huang[2#], Xiaojuan Yi[2], Youpan Tang[3], Riki Okita[4], Jun He[5]

[1]Department of Radiotherapy, The Second Affiliated Hospital of Xuzhou Medical University, Xuzhou, China; [2]Department of Clinical Medicine, Southwest Medical University, Luzhou, China; [3]Department of Gastroenterology, Zhongjiang People's Hospital, Deyang, China; [4]Department of Thoracic Surgery, National Hospital Organization Yamaguchi Ube Medical Center, Ube, Japan; [5]Department of Oncology, The Third Hospital of Mian Yang (Sichuan Mental Health Center), Mianyang, China

Contributions: (I) Conception and design: J He; (II) Administrative support: C Li; (III) Provision of study materials or patients: Y Huang; (IV) Collection and assembly of data: X Yi; (V) Data analysis and interpretation: Y Tang; (VI) Manuscript writing: All authors; (VII) Final approval of manuscript: All authors.

[#]These authors contributed equally to this work.

Correspondence to: Jun He, MD. Department of Oncology, The Third Hospital of Mian Yang (Sichuan Mental Health Center), No. 190 East Jiannan Road, Mianyang 621000, China. Email: he-001jun@163.com.

Background: Natural killer (NK) cells play a significant role in antitumor immunity and are closely related to tumor prognosis and recurrence. NK cell-based tumor immunotherapy, including immune checkpoint inhibition and CAR-engineered NK cells, is a promising area of research. However, there is a need for better NK cell-related models and associated biomarkers.

Methods: The sequences of NK cell-related genes were obtained from the published NK cell CRISPR/Cas9 library data, and the common genes were selected as NK cell-related genes. The RNA sequencing (RNA-seq) and clinical data of 32 solid tumors from The Cancer Genome Atlas (TCGA) were downloaded from the UCSC Xena database, and the RNA-seq data of normal samples were downloaded from the Genotype-Tissue Expression (GTEx) database. The differentially expressed NK cell-related genes (DENKGs) between the tumor and normal samples were analyzed. The DENKGs related to the prognosis of solid tumors were selected via univariate Cox analysis, and 32 kinds of solid tumor prognostic models were constructed using least absolute shrinkage and selection operator (LASSO) and multivariate Cox analysis. Survival, receiver operating characteristic (ROC), and independent prognostic analyses were employed to test the effectiveness of the model, along with a nomogram model and prediction curve. Differences in the immune pathways and microenvironment cells were analyzed between the high- and low-risk groups identified by the model.

Results: We constructed a pan-cancer prognostic model with 63 NK cell-related genes and further identified *DEPDC1* and *ASPM* as potentially offering new directions in tumor research by literature screening.

Conclusions: In this study, 63 prognostic solid tumor markers were investigated using NK cell-related genes, and for the first time, a pan-cancer prognostic model was constructed to analyze their role in the immune microenvironment, which may contribute new insights into tumor research.

Keywords: Natural killer cell-related genes (NK cell-related genes); pan-cancer; prognosis; *DEPDC1*; *ASPM*

Submitted Mar 17, 2024. Accepted for publication Apr 15, 2024. Published online Apr 25, 2024.
doi: 10.21037/tcr-24-434
View this article at: https://dx.doi.org/10.21037/tcr-24-434

Introduction

Natural killer (NK) cells are a type of cytotoxic lymphocytes that are essential for cancer surveillance and can act as effectors without prior sensitization (1). A study has demonstrated that infused allogeneic NK cells can safely cross the human leukocyte antigen barrier and avoid graft-versus-host disease reaction (2).

NK cell-based tumor immunotherapy, including NK cell-based immune checkpoint inhibition and CAR-engineered NK cells. Some researchers have proposed utilizing NK cells as novel targets for immune checkpoint inhibition, suggesting that the combination of anti-programmed death 1 (PD-1), anti-programmed death-ligand 1 (PD-L1) inhibitors with NK cell-specific checkpoint inhibitors may hold significant value for combination immune checkpoint therapy (3). Besides, drawing inspiration from the CAR-T immunotherapy, researchers have extended their focus to other immune cells, including CAR-NK, CAR-CIK, and CAR-MΦ. Among these, CAR-NK cells exhibit several advantages over CAR-T cells, including better safety, superior antitumor activity, and high efficiency for 'off-the-shelf' manufacturing (4-6).

Highlight box

Key findings

- The research developed a pan-cancer prognostic model using 63 genes related to natural killer (NK) cells. By screening the literature, *DEPDC1* and *ASPM* were identified as potential areas for new tumor research.

What is known and what is new?

- NK cells play a significant role in antitumor immunity and are closely related to tumor prognosis and recurrence.
- A pan-cancer prognostic model was constructed with 63 NK cell-related genes and further identified two genes, *DEPDC1* and *ASPM*, which were not reported to be associated with NK cell killing in previous studies.

What is the implication, and what should change now?

- In this paper, a pan-cancer prognostic model was constructed to analyze their role in the immune microenvironment, which may contribute new insights into tumor research.
- Two genes, *DEPDC1* and *ASPM*, were further identified. By reviewing the literature, it is found that the possible associations of ASPM with thymoma and uveal melanoma have not yet been reported. Furthermore, there exists some disagreement about the relationship between *DEPDC1* expression and the prognosis of stomach adenocarcinoma, which remains to be further explored in future studies.

A recent study demonstrates utilization of the nanotechnology in NK cell-based tumor immunotherapy. However, the full realization of engineered NK cells' potential in clinical practice has been hindered by the absence of suitable models to comprehensively study human NK cell biology complexity (7). Additionally, it has been emphasized that to maximize patient benefits from immunotherapy, personalized analysis of cancer based on biomarkers are of paramount importance (3). Hence, there is an urgent need to develop NK cell-related models or identify associated biomarkers through diverse approaches. In this study, we construct a pan-cancer prognostic model based on 63 NK cell-related genes and screened two key genes, *ASPM* and *DEPDC1*, which may provide a new direction for future study to further analyze of the mechanisms underlying NK cell-mediated tumor immunity and lay the foundation for personalized drug development. We present this article in accordance with the TRIPOD reporting checklist (available at https://tcr.amegroups.com/article/view/10.21037/tcr-24-434/rc).

Methods

Data download and preprocessing

The CRISPR/Cas9 library data related to NK cell killing were obtained from the literature (8-10), and the intersection was obtained via Venn diagram analysis (11). RNA sequencing (RNA-seq) [fragments per kilobase per million (FPKM) value] and the clinical data of 32 cancers from The Cancer Genome Atlas (TCGA) database were downloaded from the USCS Xena database (https://xena.ucsc.edu/), RNA-seq data (FPKM value) of normal tissues were downloaded from the GTEx database (https://gtexportal.org/home/), and pan-cancer prognostic data were downloaded from the Gene Expression Omnibus (GEO) database (https://www.ncbi.nlm.nih.gov/gds). The study was conducted in accordance with the Declaration of Helsinki (as revised in 2013). The normalizeBetweenArrays algorithm in the "limma" R package (The R Foundation for Statistical Computing) (12) was used to correct the data.

Differentially expressed NK cells associated with tumor prognosis

We first extracted information on the messenger RNA (mRNA) expressions of NK cell-related genes from the RNA-seq data obtained from the GTEx and TCGA

databases, analyzed the differences in these genes between the tumor and normal samples using the Wilcoxon test, and determined the common differentially expressed NK cell-related genes (DENKGs) in different tumors using the "RobustRankAggreg" R package (13). Univariate Cox analysis was employed to screen the prognosis-related DENKGs for solid tumors.

Prognostic model of NK cells in solid tumors

We used the "glmnet" R package (14) to screen the overfitted prognosis-related DENKGs via least absolute shrinkage and selection operator (LASSO) regression, and the prognostic model of NK cells in solid tumors was constructed via multivariate Cox analysis. Furthermore, the data were randomly categorized into training and test groups at a ratio of 8:2 for model verification. Additionally, six different cancer datasets from GEO were used to further validate our prognostic model.

Nomogram model

The "survival" R package (15) was used to conduct survival curve and receiver operating characteristic (ROC) analyses of the model, and independent prognostic analysis was employed to verify the effectiveness of the model. In addition, a nomogram model of solid tumor prognosis was constructed, and the nomogram calibration curve was used to test its prognostic effect. ROC and concordance index (C-index) were also used to analyze the accuracy of the nomogram model.

Analysis of the immune microenvironment

TCGA pan-cancer samples were classified into high- and low-risk groups according to the risk model. The "GSEA" R package (16) was used to analyze the enriched immune pathways in the high- and low-risk groups so as to verify the enrichment effect of the immune pathways on the model. The proportion of immune cells in pan-cancer samples was analyzed using the "CIBERSORT" R package (17), and the difference of immune cells between the high- and low-risk groups was analyzed.

Analysis of tumor mutational burden (TMB)

To characterize the differences in tumor mutation between the high- and low-risk groups, we downloaded pan-cancer mutation data from UCSC Xena, calculated the TMB using the Perl script, and categorized the patients into two groups. Furthermore, we separately analyzed the differences in the TMB value between the high- and low-risk groups.

Gene analysis of the NK cell prognostic model

First, the interactions between the genes in the model were analyzed using the Search Tool for the Retrieval of Interacting Genes/Proteins (STRING) (18) database (https://cn.string-db.org/), and those with binding scores >0.7 were selected as the core genes. Second, the relationship between core genes and immune microenvironment and stem cell scoring was further analyzed using the "CIBERSORT" R package (19). Prognostic survival analysis was also employed as an important method for core gene screening.

Statistical analysis

Data are presented as means ± standard error of the mean (SEM). Wilcoxon test was applied to analyze the differences of NK cell-related genes between the tumor and normal samples according to the TCGA and GTEx database. Statistical analyses were performed using R 4.1.2. $P<0.05$ was considered statistically significant. A Perl script was used to calculate the TMB value.

Results

Differential and prognostic NK cell-related genes

The design and process of our study are presented in *Figure 1*. Five CRISPR/Cas9 library results were obtained from the studies conducted by Kearney *et al.* (8), Freeman *et al.* (9), and Sheffer *et al.* (10). A total of 771 NK cell-related genes were obtained via Venn diagram analysis performed to determine the intersection of ≥ two datasets, which were found to be valid (*Figure 2A*,*2B*). After the combination of the TCGA and GTEx data, the differences in the 730 NK cell-related genes between tumor and control samples were tested. A total of 184 DENKGs were screened using the "RobustRankAggreg" R package (13) (*Figure 2C*). Univariate Cox analysis was employed to screen 136 DENKGs related to pan-cancer prognosis (*Table 1*).

DENKG prognostic risk model

After the overfitted DENKGs were screened via LASSO

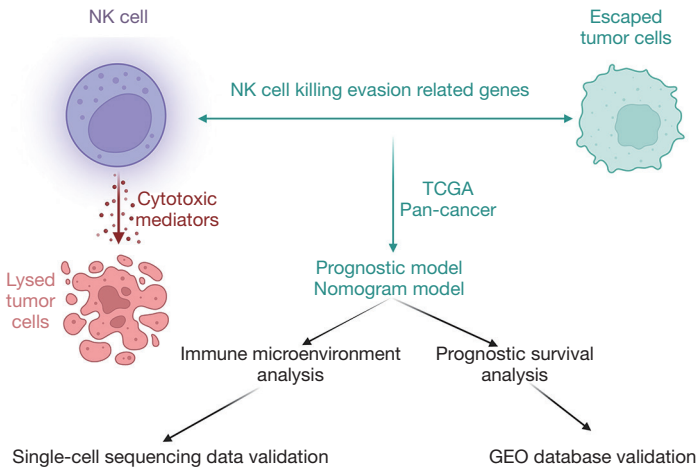

Figure 1 Visualization of the study concept. NK, natural killer; GEO, Gene Expression Omnibus; TCGA, The Cancer Genome Atlas.

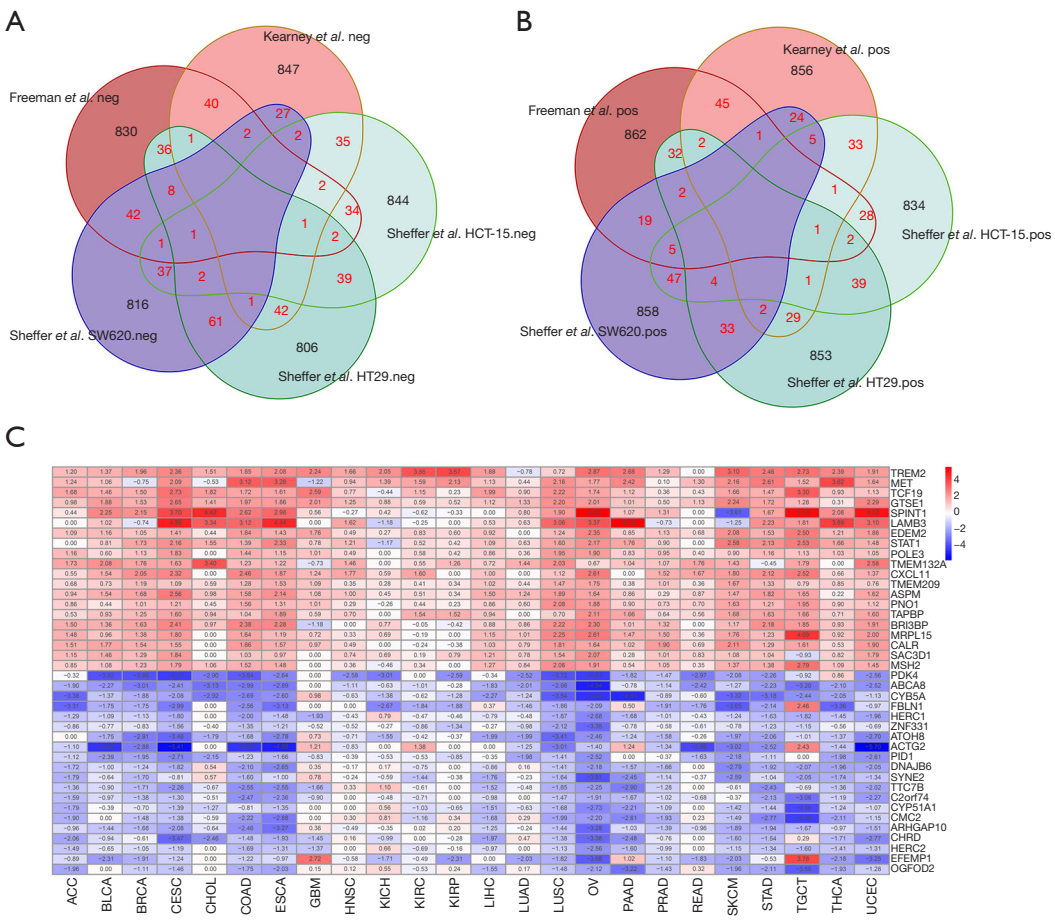

Figure 2 Recognition of differential NK cell-related genes. (A,B) Venn diagrams illustrating the process of obtaining 771 NK cell-related genes. (C) Pan-cancer differential heatmap of differentially expressed NK cell-related genes after combined examination. The color scale of the heat map is the z-score score of the RNA-seq sequencing data. neg, negative; pos, positive; ACC, adrenocortical carcinoma; BLCA, bladder urothelial carcinoma; BRCA, breast invasive carcinoma; CESC, cervical squamous cell carcinoma and endocervical adeno carcinoma;

CHOL, cholangiocarcinoma; COAD, colon adenocarcinoma; ESCA, esophageal carcinoma; GBM, glioblastoma multiforme; HNSC, head and Neck squamous cell carcinoma; KICH, kidney chromophobe; KIRC, kidney renal clear cell carcinoma; KIRP, kidney renal papillary cell carcinoma; LIHC, liver hepatocellular carcinoma; LUAD, lung adenocarcinoma; LUSC, lung squamous cell carcinoma; OV, ovarian serous cystadenocarcinoma; PAAD, pancreatic adenocarcinoma; PRAD, prostate adenocarcinoma; PEAD, rectum adenocarcinoma; SKCM, skin cutaneous melanoma; STAD, stomach adenocarcinoma; TGCT, testicular germ cell tumors; THCA, thyroid carcinoma; UCEC, uterine corpus endometrial carcinoma; NK, natural killer; RNA-seq, RNA-sequencing.

Table 1 Univariate Cox analysis of natural killer cell-related genes in pan-cancer

Gene	HR	HR 95L	HR 95H	P value
ASPM	1.765335	1.64416	1.89544	2.63E–55
CRY2	0.300167	0.25784	0.34944	2.66E–54
DEPDC1	1.726787	1.60937	1.85277	3.33E–52
SNX1	0.176422	0.14077	0.2211	2.79E–51
TMEM158	1.614313	1.51535	1.71974	8.43E–50
GTSE1	1.747023	1.62188	1.88182	5.37E–49
LRRC27	0.391062	0.34329	0.44548	2.74E–45
MSANTD3	3.782003	3.13263	4.56599	1.46E–43
E2F8	1.629834	1.52008	1.74751	6.44E–43
ZIC2	1.396849	1.32864	1.46856	4.03E–39
B4GALT5	3.647815	3.00407	4.42951	5.31E–39
CFAP69	0.448298	0.39738	0.50574	6.93E–39
SRXN1	1.77672	1.62956	1.93717	8.34E–39
HERC1	0.334825	0.28332	0.39569	9.93E–38
SLC35C1	2.903049	2.46438	3.4198	3.08E–37
CRBN	0.297112	0.24494	0.3604	7.18E–35
KANK3	0.558185	0.50789	0.61347	1.04E–33
TCF19	1.947962	1.73628	2.18545	6.58E–30
WDR20	0.264804	0.21015	0.33367	1.92E–29
NRBF2	4.169672	3.21529	5.40734	4.94E–27
CDC7	1.696141	1.54023	1.86783	6.61E–27
SYNE2	0.525487	0.46596	0.59263	9.76E–26
LMF1	0.561003	0.50312	0.62555	2.39E–25
PNO1	3.388568	2.65755	4.32067	7.32E–23
TMEM132A	1.576354	1.43967	1.72601	7.96E–23
ANXA6	0.541267	0.47693	0.61429	1.97E–21
ERCC5	0.448042	0.37941	0.52908	2.94E–21
CCDC71	0.341456	0.27282	0.42736	6.29E–21
NMRK1	0.537575	0.47142	0.61301	1.96E–20
LAMB3	1.303835	1.22995	1.38216	4.94E–19
RAC1	6.708947	4.39132	10.2498	1.34E–18
ATOH8	0.759045	0.71341	0.8076	2.92E–18
DNTTIP1	2.82242	2.23025	3.57182	5.81E–18
BRIP1	1.439142	1.32391	1.56441	1.24E–17
ARF3	0.240691	0.17233	0.33618	6.58E–17
DLG2	0.63909	0.57383	0.71176	3.72E–16
LUC7L2	0.311179	0.2349	0.41223	4.07E–16
THBS3	1.748406	1.52642	2.00267	7.32E–16
PDK4	0.788456	0.74393	0.83565	1.11E–15
TRAF7	2.762126	2.15155	3.54598	1.57E–15
PPIL1	2.558938	2.03091	3.22425	1.61E–15
IKZF3	0.757816	0.70736	0.81187	3.04E–15
UACA	0.617324	0.54721	0.69642	4.43E–15
PRR15L	0.861562	0.82994	0.89438	5.67E–15
PEG3	0.787961	0.74086	0.83805	3.49E–14
CCAR2	0.399318	0.31483	0.50648	3.77E–14
TSEN15	2.341763	1.86901	2.9341	1.41E–13
CMYA5	0.741102	0.68439	0.80252	1.63E–13
ZNF331	0.674646	0.6074	0.74934	2.03E–13
RELB	1.63665	1.43324	1.86893	3.45E–13
AP1M1	1.948639	1.62797	2.33247	3.53E–13
DMGDH	0.779652	0.72862	0.83426	5.73E–13
C1QTNF1	1.412917	1.28567	1.55276	7.06E–13
GTF2H3	2.453881	1.92031	3.13571	7.19E–13
MRPL15	2.507044	1.94514	3.23128	1.26E–12
CDK5RAP3	0.480827	0.39191	0.58992	2.24E–12
PITPNM2	1.439583	1.29924	1.59509	3.36E–12
BCAN	1.149548	1.10369	1.19731	1.95E–11
EDEM2	2.480786	1.89159	3.2535	5.12E–11
MOB1A	2.455448	1.87707	3.21204	5.56E–11
EXD3	0.660047	0.58233	0.74813	8.02E–11

Table 1 *(continued)*

Gene	HR	HR 95L	HR 95H	P value
OXTR	1.264809	1.17689	1.3593	1.65E−10
VEGFA	1.339791	1.22426	1.46622	2.05E−10
DNAJB6	1.950501	1.57684	2.41271	7.40E−10
ITPKC	1.751919	1.46413	2.09628	9.12E−10
SAC3D1	1.483356	1.30664	1.68398	1.11E−09
POLE3	2.436907	1.82458	3.25474	1.61E−09
SLC35A2	1.980095	1.58576	2.47248	1.65E−09
C2orf74	0.780065	0.719329	0.84593	1.90E−09
CYP51A1	1.345769	1.220756	1.48359	2.37E−09
FBLN1	1.230317	1.148977	1.31741	2.86E−09
BRI3BP	1.506361	1.315343	1.72512	3.18E−09
STK4	1.891211	1.528935	2.33933	4.27E−09
PYGO2	0.451677	0.341712	0.59703	2.36E−08
EFEMP1	1.238168	1.148672	1.33464	2.39E−08
IKBKG	1.491816	1.292539	1.72182	4.56E−08
CD34	0.752885	0.677572	0.83657	1.30E−07
PFKFB4	1.30387	1.180117	1.4406	1.84E−07
HFM1	0.671015	0.577273	0.77998	2.03E−07
TREM2	1.253687	1.151075	1.36545	2.11E−07
SHC2	0.836544	0.781848	0.89507	2.30E−07
SCAMP5	0.793343	0.726576	0.86624	2.45E−07
PID1	1.168711	1.100984	1.2406	3.08E−07
MET	1.163761	1.097253	1.2343	4.39E−07
PDP1	0.718749	0.632071	0.81731	4.74E−07
DDR2	1.211411	1.123883	1.30576	5.38E−07
ME3	0.813547	0.749458	0.88312	8.26E−07
TAP1	1.43316	1.241208	1.6548	9.33E−07
NDEL1	1.685718	1.355619	2.0962	2.65E−06
PDCL	0.53852	0.414899	0.69897	3.29E−06
ARHGAP10	0.769212	0.68814	0.85984	3.88E−06
CYB5A	0.810169	0.738754	0.88849	7.78E−06
HERC2	0.667784	0.555699	0.80248	1.65E−05
SOX10	5.64E−36	2.26E−52	1.41E−19	2.52E−05
GP1BB	5.64E−36	2.26E−52	1.41E−19	2.52E−05
DAZAP2	0.500619	0.358446	0.69918	4.92E−05
TM9SF2	0.554394	0.415449	0.73981	6.14E−05
MZF1	0.767031	0.67355	0.87349	6.34E−05

Table 1 *(continued)*

Table 1 *(continued)*

Gene	HR	HR 95L	HR 95H	P value
CC2D2A	0.805539	0.723826	0.89648	7.42E−05
SPINT1	0.904722	0.860319	0.95142	9.64E−05
MYL3	0.869839	0.810814	0.93316	0.0001
GRB2	0.488561	0.338547	0.70505	0.000129
CDK10	0.752894	0.650412	0.87152	0.000144
POLR1B	1.438897	1.19174	1.73731	0.000154
STAT1	1.357285	1.153264	1.5974	0.000237
TMEM81	1.304715	1.131917	1.50389	0.000243
CLIP4	1.161742	1.070908	1.26028	0.000307
MAP3K12	1.210209	1.090331	1.34327	0.000337
NIF3L1	1.671069	1.24791	2.23772	0.000568
YDJC	1.239501	1.093703	1.40473	0.000772
LEO1	0.667489	0.525121	0.84845	0.000958
SON	0.645861	0.491231	0.84917	0.001743
PLIN2	1.145417	1.049574	1.25001	0.002325
CNBD2	0.629512	0.463982	0.8541	0.002948
SLC35B3	0.692636	0.538824	0.89035	0.004152
ABCA8	0.901293	0.839446	0.9677	0.004166
TMEM209	1.355676	1.099138	1.67209	0.004467
ASPG	1.100884	1.028925	1.17788	0.005325
NOP10	1.617456	1.135009	2.30497	0.007798
AKAP12	1.101045	1.025406	1.18226	0.008029
MBD2	0.749007	0.604766	0.92765	0.008095
TRAF2	0.785976	0.657473	0.93959	0.008193
PSMB3	1.516803	1.110832	2.07114	0.008759
ARHGAP24	0.900004	0.831823	0.97377	0.008763
IFNGR2	1.403803	1.082233	1.82092	0.010609
HSPA4	0.670607	0.48797	0.9216	0.013767
RNF31	1.255841	1.04685	1.50655	0.014168
UGP2	1.346234	1.058687	1.71188	0.015302
LTC4S	0.701113	0.524051	0.938	0.016805
SPTBN1	1.227038	1.034371	1.45559	0.018888
MICAL3	1.126359	1.01696	1.24753	0.022455
UNG	1.295687	1.036186	1.62018	0.023105
ZBTB12	1.123996	1.010022	1.25083	0.032132
TMEM87B	0.860211	0.747686	0.98967	0.03528
NAALAD2	0.873619	0.766974	0.99509	0.041947
SAMD4A	1.096398	1.000643	1.20132	0.04841

HR, hazard ratio; 95L, lower limit of 95% confidence interval; 95H, higher limit of 95% confidence interval.

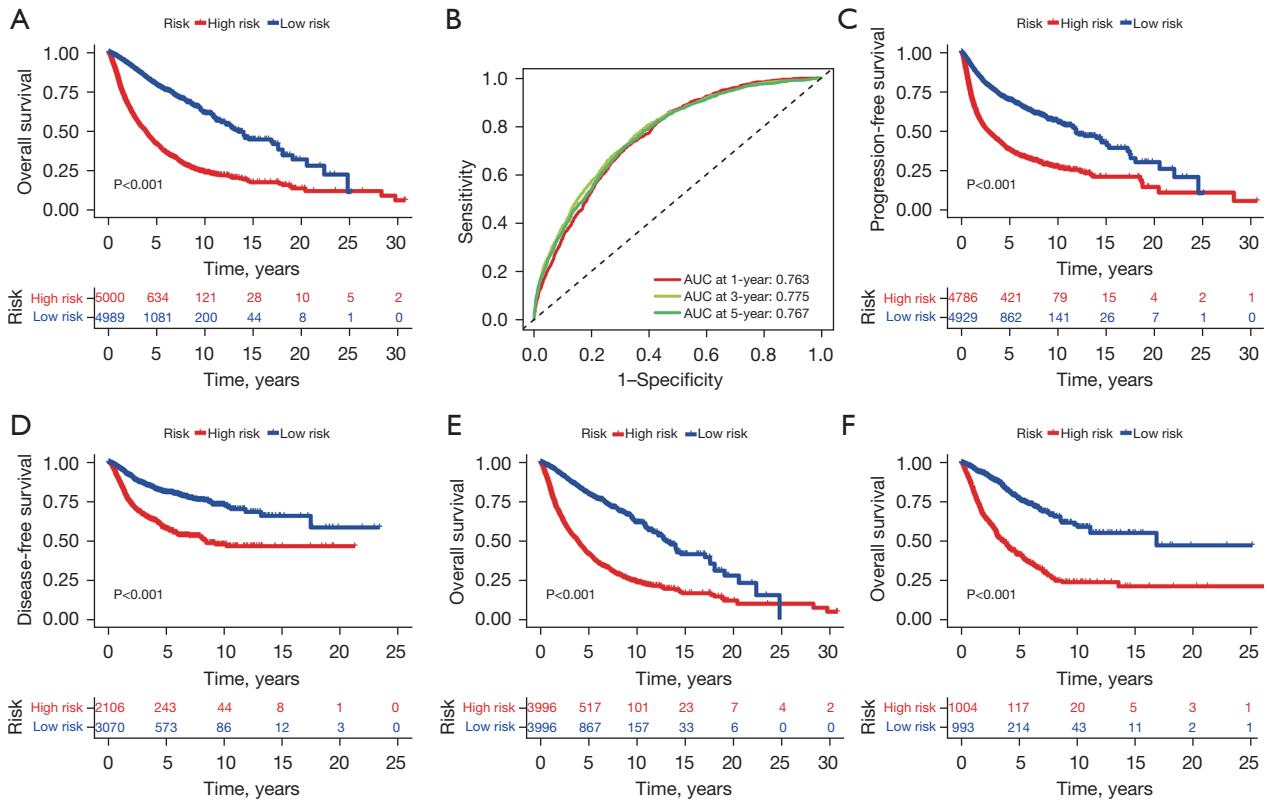

Figure 3 Prognostic risk model test of pan-cancer. (A) Analysis of the total survival time of patients in the high- and low-risk groups in the prognostic model. (B) Receiver operating characteristic curve of the 1-, 3-, and 5-year AUC value for testing the model. (C,D) Kaplan-Meier curves of progression-free survival and disease-free survival in the high- and low-risk groups. (E,F) Survival analysis of the high- and low-risk groups of both the training and validation groups for further verifying the model. AUC, area under the curve.

regression, multifactor Cox analysis was employed to construct the risk model. Furthermore, 63 prognostic genes (Table S1) were identified via multivariate Cox analysis and were used to construct a pan-cancer prognostic risk model according to the following risk formula: (expressing gene1 × β gene1) + (expressing gene2 × β gene2). In addition, the pan-cancer samples from TCGA were randomly categorized into groups at a ratio of 8:2 to test the effectiveness of the model.

Testing the prognostic risk model for pan-cancer

Survival and ROC analyses revealed that our model could well predict tumor prognosis (*Figure 3A,3B*), disease progression, and recurrence (*Figure 3C,3D*). This finding was also verified in the survival analysis of both the training and validation groups (*Figure 3E,3F*). Independent prognostic analysis was performed on age, sex, cancer stage, and risk score. Multivariate and univariate independent prognostic analyses revealed that our risk score could predict tumor prognosis independently of other clinical data (*Figure 4A,4B*).

Nomogram model

To further study the prognosis of pan-cancer, we constructed a nomogram model (*Figure 4C*) and used the nomogram (*Figure 4D*) and ROC curve (*Figure 4E*) to verify the effectiveness of the model. The line chart and ROC curve demonstrated that our model was effective, and the C-index (*Figure 4F*) was >0.7, which was ideal.

Analysis of the immune microenvironment

The enrichment of immune pathways showed that there were differences in most immune pathways between the high- and low-risk groups of our model (*Figure 5A*).

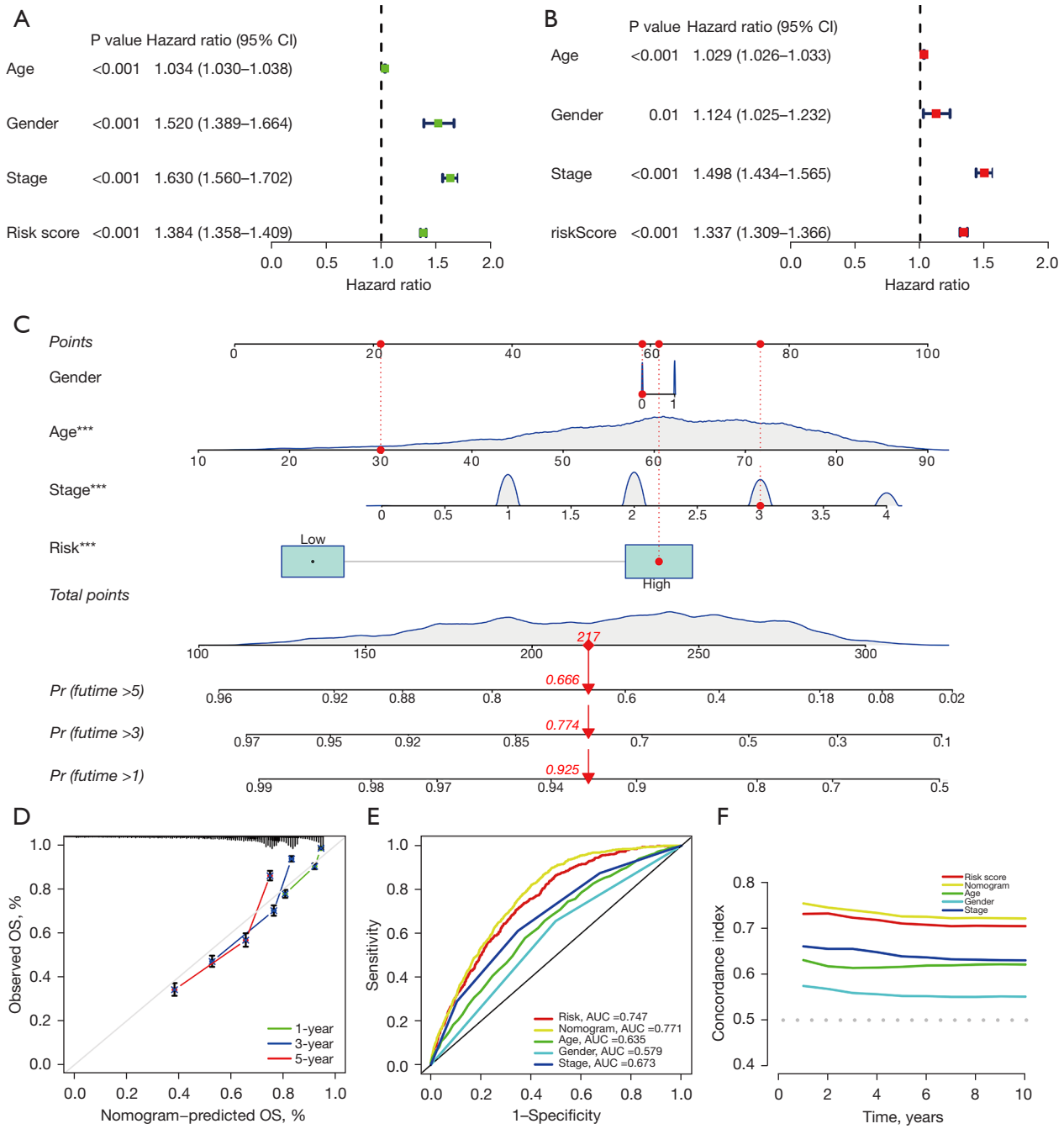

Figure 4 Clinical analysis of the prognostic characteristics of natural killer cell-related genes. (A) Univariate Cox regression analysis of the clinical features and signature-based risk scores. (B) Multivariate Cox regression analysis. (C) Nomogram for predicting the 1-, 3-, and 5-year survival rates of patients. (D) Nomogram correction curve of the predicted OS for 1, 3, and 5 years. (E,F) Receiver operating characteristic curve and concordance index chart of clinical features and signature-based risk scores, respectively. ***, P<0.001. CI, confidence interval; OS, overall survival; Pr, probability; AUC, area under the curve.

These differences were analyzed using the CIBERSORT algorithm (19). As can be seen from the *Figure 5B*, our model was different in most immune cells. To further understand the relationship between NK cells and tumor prognosis, we analyzed the survival of resting and activated NK cells for pan-cancer prognosis, and activated NK cells predicted according to the algorithm cells were found to be associated with good tumor prognosis (*Figure 5C,5D*).

Analysis of TMB

The higher the TMB value is, the worse the tumor prognosis. We obtained pan-cancer mutation data from TCGA database and determined the correlation between pan-cancer TMB and the high- and low-risk groups of the model. Then we testified the accuracy of our model and classified each tumor to analyze the correlation between TMB and risk score and drew a radar map (*Figure 5E,5F*).

Prognostic core genes of pan-cancer NK cells

A total of 63 prognosis-related DENKGs from the STRING database were included to analyze the protein-protein relationship. A protein-protein interaction (PPI) network map was established and visualized using the Cytoscape software (version 3.9.1) (*Figure 6A*). Genes with a binding coefficient of ≥0.7 were selected as the core genes and were displayed in a correlation analysis map (*Figure 6B*).

Analysis of the immune microenvironment and prognosis of core genes

The expression values of the above-mentioned core genes in various tumors were correlated with immune, stromal, and stem cell scores, and the related heat map was created (*Figure 6C-6F*). The immune and stromal scores were negatively correlated with the expression levels of the core genes (*Figure 6C,6D*). Conversely, a significant positive correlation existed between the expression of the core genes and RNA stemness scores (RNAss) (*Figure 6E*). A total of 15 core genes were linked to tumor prognostic data, and the gene survival curves in each tumor were drawn to further screen the pan-cancer related genes that were linked to prognosis in NK cells. Among the 15 core genes, *ASPM* and *DEPDC1* were found to play a key role in the prognosis of 12 and 14 tumor types, respectively (*Table 2*). It is noteworthy to highlight that high *DEPDC1* gene expression was associated with better prognosis of colon adenocarcinoma (COAD), stomach adenocarcinoma (STAD), rectum adenocarcinoma (READ) and thymoma (THYM), whereas low *DEPDC1* gene expression was associated with better prognosis in ten other types of cancer (*Figure 7*, Figure S1). In addition, five different tumor types were collected in GEO database to verify our findings (*Figure 8*). We also observed that the expression of *DEPDC1* varied in its correlation with activated and resting NK cells across different cancer types (Figure S2).

Discussion

PD-L1 inhibitors have been approved by the US Food and Drug Administration (FDA) for the treatment of melanoma, lung cancer, and other diseases, and their application in immunotherapy has made a significant progress (20); however, immunotherapy is not effective in all tumors (21), and this limitation has spurred research into identifying the reasons underlying this lack of efficacy and into developing new therapeutic approaches.

NK cells are innate immune-related lymphocytes, which also play a particularly significant role in antitumor immunity (22). NK cell-based tumor immunotherapy, including immune checkpoint inhibition and CAR-engineered NK cells, is a promising area of research. However, there is a need for better NK cell-related models and associated biomarkers. Thus, we conducted a pan-cancer analysis focusing on the role of NK cell-related genes in pan-cancer. However, in comparison with other studies, the NK cell-related genes used in the present study were not obtained from the Kyoto Encyclopedia of Genes and Genomes (KEGG) database. Considering that there are still unknown NK cell-related genes to be mined, we selected the library of CRISPR/Cas9, a gene-editing technology which enables large-scale and in-depth sequencing (23), for analysis.

Because the library was sequenced *in vitro*, 14,148 samples were used from TCGA and GTEx pan-cancer data to analyze the expressions of the aforementioned genes in the tumor and control samples. After the DENKGs were analyzed, a pan-cancer prognostic model was constructed with 63 NK cell-related genes via univariate and multivariate Cox analyses. Based on the ROC results, the model had a 1-year area under the curve (AUC) value of 0.747 for predicting tumor prognosis, which was higher than that based on tumor staging (1-year AUC =0.673). The C-index of the model was >0.7, thus confirming its value in the study of pan-cancer prognosis. The high- and low-risk grouping of the prognostic model was verified through

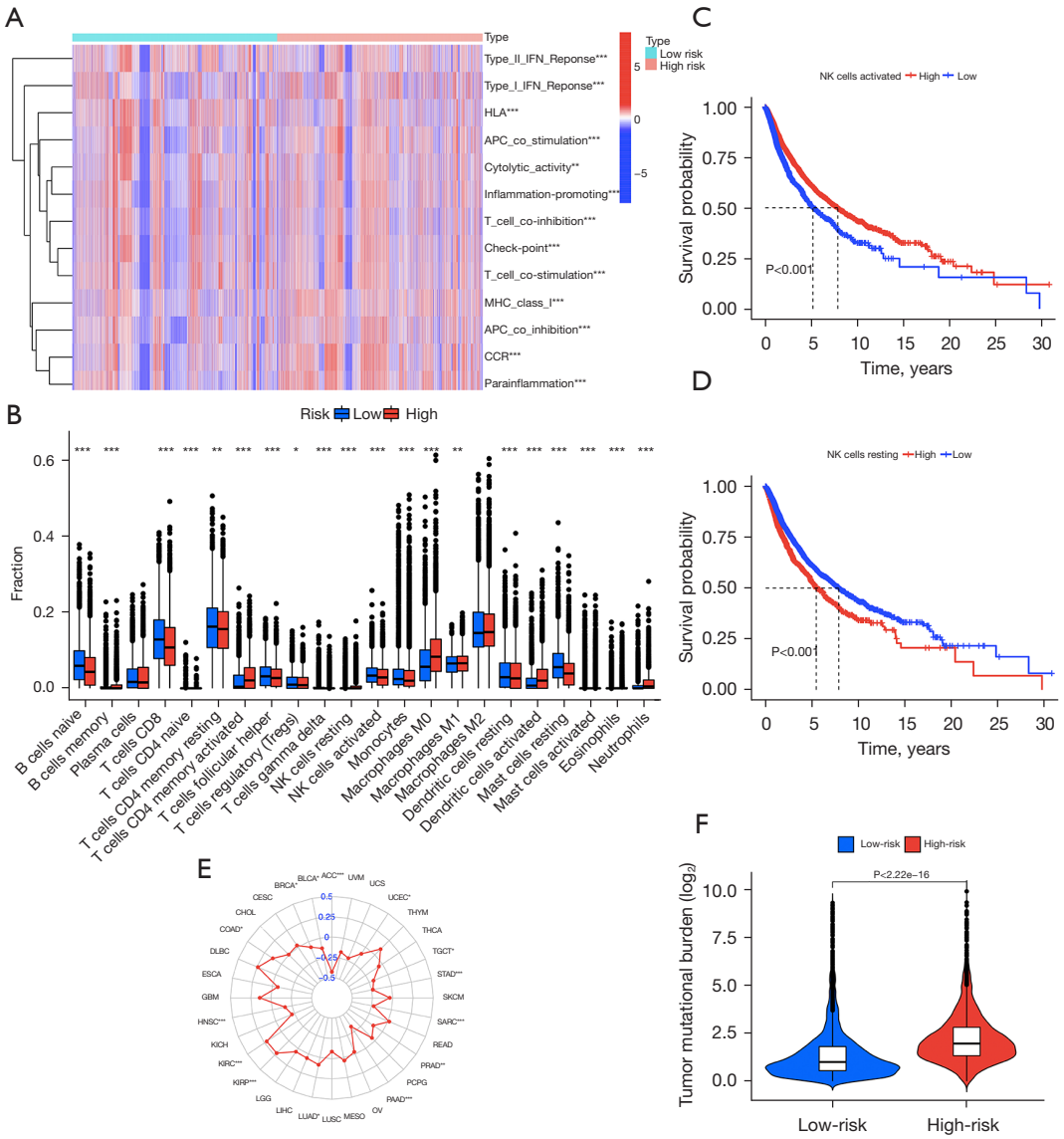

Figure 5 Immune microenvironment and tumor mutational burden analyses of prognostic characteristics. (A) Heatmap of the differential enrichment of immune-related pathways in the high- and low-risk groups of the prognostic models. The color scale of the heat map is the z-score score of the RNA-seq sequencing data. (B) Composition of immune infiltration in the high- and low-risk groups. (C,D) Kaplan-Meier survival curves of resting NK cells, activated NK cells, and pan-cancer prognosis in the high- and low-risk groups, respectively. (E) Correlation between tumor mutational burden and risk score. (F) Violin plot of tumor mutational burden in the high- and low-risk groups. *, P<0.05; **, P<0.01; ***, P<0.001. IFN, interferon; HLA, human leukocyte antigen; APC, antigen-presenting cells; MHC, major histocompatibility complex; CCR, C-C chemokine receptor; NK, natural killer; ACC, adrenocortical carcinoma; BLCA, bladder urothelial carcinoma; BRCA, breast invasive carcinoma; CESC, cervical squamous cell carcinoma and endocervical adenocarcinoma; CHOL, cholangiocarcinoma; COAD, colon adenocarcinoma; DLBC, lymphoid neoplasm diffuse large B-cell lymphoma; ESCA, esophageal carcinoma; GBM, glioblastoma multiforme; HNSC, head and neck squamous cell carcinoma; KICH, kidney chromophobe; KIRC, kidney renal clear cell carcinoma; KIRP, kidney renal papillary cell carcinoma; LGG, brain lower grade glioma; LIHC, liver hepatocellular carcinoma; LUAD, lung adenocarcinoma; LUSC, lung squamous cell carcinoma; MESO, mesothelioma; OV, ovarian serous cystadenocarcinoma; PAAD, pancreatic adenocarcinoma; PCPG, pheochromocytoma and paraganglioma; PRAD, prostate adenocarcinoma; READ, rectum adenocarcinoma; SARC, sarcoma; SKCM, skin cutaneous melanoma; STAD, stomach adenocarcinoma; TGCT, testicular germ cell tumors; THCA, thyroid carcinoma; THYM, thymoma; UCEC, uterine corpus endometrial carcinoma; UCS, uterine carcinosarcoma; UVM, uveal melanoma; RNA-seq, RNA-sequencing.

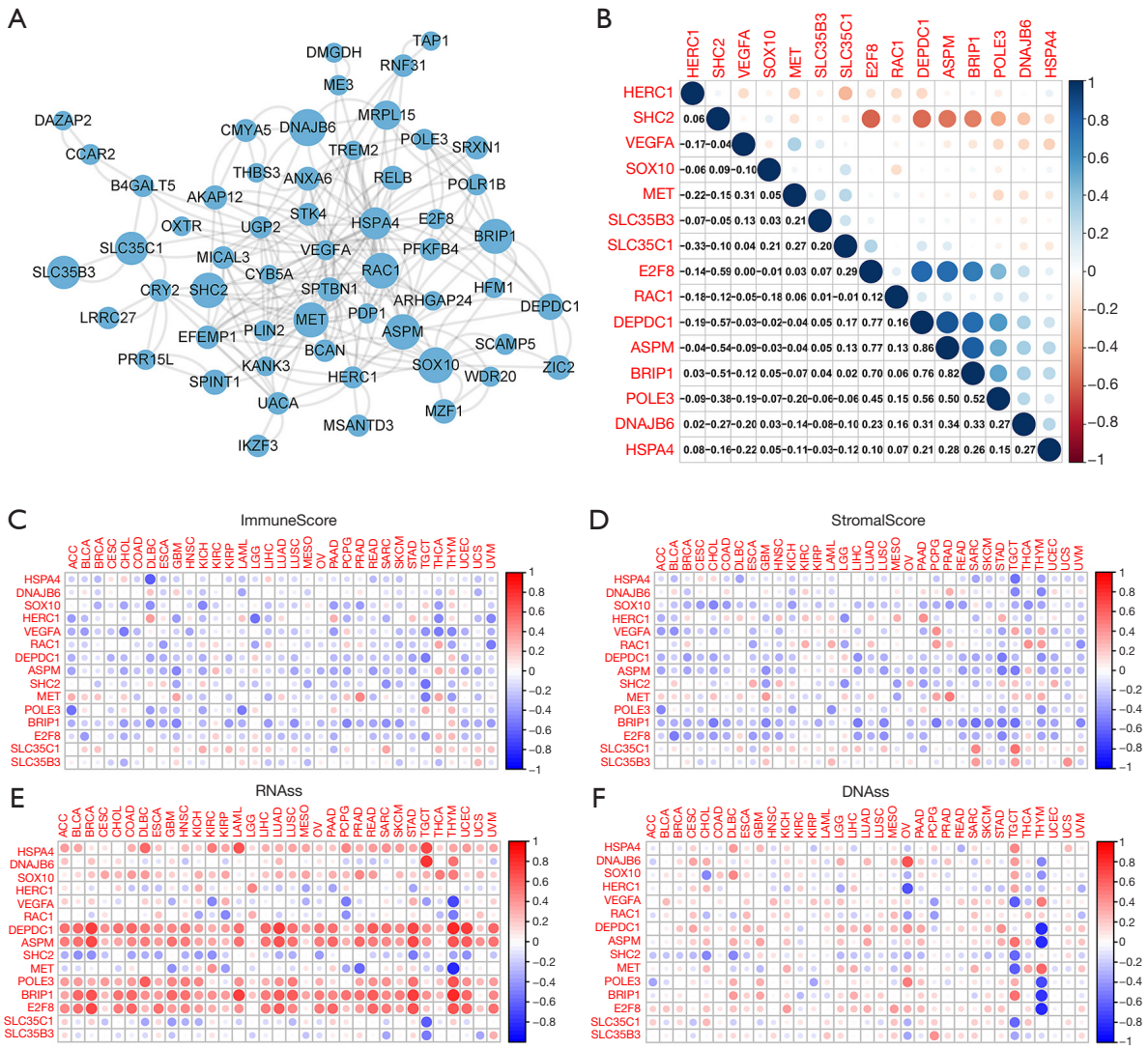

Figure 6 Screening of core genes for the prognosis of pan-cancer NK cells and their immune microenvironment. (A) The protein-protein interaction network diagram of 63 prognosis-related differentially expressed NK cell-related genes. (B) Correlation heatmap of 15 core genes from further screening. (C,D) Correlation between the immune and stromal scores and the 15 core genes in pan-cancer. (E) Correlation between the 15 core genes and pan-cancer RNA stem cell score. (F) Correlation between pan-cancer RNA stem cell score and pan-cancer DNA stem cell score. The color scale of the heat map is the z-score of the RNA-seq sequencing data. RNAss, RNA stemness score; DNAss, DNA stemness score; ACC, adrenocortical carcinoma; BLCA, bladder urothelial carcinoma; BRCA, breast invasive carcinoma; CESC, cervical squamous cell carcinoma and endocervical adenocarcinoma; CHOL, cholangiocarcinoma; COAD, colon adenocarcinoma; DLBC, lymphoid neoplasm diffuse large B-cell lymphoma; ESCA, esophageal carcinoma; GBM, glioblastoma multiforme; HNSC, head and neck squamous cell carcinoma; KICH, kidney chromophobe; KIRC, kidney renal clear cell carcinoma; KIRP, kidney renal papillary cell carcinoma; LAML, acute myeloid leukemia; LGG, brain lower grade glioma; LIHC, liver hepatocellular carcinoma; LUAD, lung adenocarcinoma; LUSC, lung squamous cell carcinoma; MESO, mesothelioma; OV, ovarian serous cystadenocarcinoma; PAAD, pancreatic adenocarcinoma; PCPG, pheochromocytoma and paraganglioma; PRAD, prostate adenocarcinoma; READ, rectum adenocarcinoma; SARC sarcoma; SKCM, skin cutaneous melanoma; STAD, stomach adenocarcinoma; TGCT, testicular germ cell tumors; THCA, thyroid carcinoma; THYM, thymoma; UCEC, uterine corpus endometrial carcinoma; UCS, uterine carcinosarcoma; UVM, uveal melanoma; NK, natural killer; RNA-seq, RNA-sequencing.

Table 2 Survival analysis of 15 core natural killer cell-related genes in pan-cancer

Gene	Cancer type	P value
HERC1	KIRC	1.46E−06
	LGG	9.58E−06
	LIHC	0.045917
	UVM	0.003986
DNAJB6	CESC	0.018468
	OV	0.01384
	SKCM	0.029439
	UCEC	0.00546
SHC2	ACC	0.010142
	CESC	0.048921
	KICH	0.02189
	LGG	0.000556
	OV	0.005896
	SKCM	0.035547
SOX10	KIRC	0.003434
	LIHC	0.03873
VEGFA	BLCA	0.018589
	CESC	0.006546
	KIRP	0.000228
	LGG	0.001337
	PRAD	0.026486
	SARC	0.025041
	UCEC	0.039948
MET	ACC	0.027873
	LGG	0.000381
	PAAD	9.42E−05
	UVM	0.016287
POLE3	ACC	0.00025
	ESCA	0.02957
	THYM	0.028938
ASPM	ACC	4.00E−09
	KIRC	0.000205
	KIRP	0.000217
	LGG	6.97E−08
	LIHC	0.006928
	LUAD	0.015197
	MESO	0.002203
	PAAD	0.043426
	PCPG	0.007278
	THYM	0.016468
	UCEC	0.00157
	UVM	0.047649
E2F8	BLCA	0.048864
	KIRC	0.002008
	KIRP	0.000346
	LGG	0.000236
	LIHC	1.64E−06
	MESO	0.000717
	PAAD	0.044548
	PCPG	0.032873
	STAD	0.003008
	THYM	0.019958
DEPDC1	ACC	2.32E−05
	COAD	0.049063
	KIRC	0.015496
	KIRP	0.000238
	LGG	6.99E−08
	LIHC	0.000543
	LUAD	0.012019
	MESO	2.40E−05
	PAAD	0.010571
	PCPG	0.006069
	READ	0.027713
	STAD	0.027779
	THYM	0.007332
	UVM	0.039939
BRIP1	ACC	0.020404
	COAD	0.017831
	KIRP	0.014144
	LGG	5.95E−05
	LUAD	0.014512

Table 2 *(continued)*

Gene	Cancer type	P value
	MESO	1.74E−06
	PAAD	0.014325
	READ	0.00895
	THYM	0.019396
SLC35C1	COAD	0.0358
	PCPG	0.030677
	STAD	0.045321
SLC35B3	READ	0.002272
	SARC	0.003276
	THCA	0.027777
	THYM	0.024145
HSPA4	LUAD	0.046428
	SARC	0.030118
	SKCM	0.011044
	STAD	0.047031
RAC1	ACC	0.008144
	DLBC	0.021017
	GBM	0.000632
	KIRC	0.002018
	LGG	0.006966
	LIHC	0.001216
	MESO	0.002586
	PCPG	0.02042
	SKCM	0.041701
	UVM	0.012914

ACC, adrenocortical carcinoma; BLCA, bladder urothelial carcinoma; BRCA, breast invasive carcinoma; CESC, cervical squamous cell carcinoma and endocervical adenocarcinoma; COAD, colon adenocarcinoma; DLBC, lymphoid neoplasm diffuse large B-cell lymphoma; ESCA, esophageal carcinoma; GBM, glioblastoma multiforme; KICH, kidney chromophobe; KIRC, kidney renal clear cell carcinoma; KIRP, kidney renal papillary cell carcinoma; LAML, acute myeloid leukemia; LGG, brain lower grade glioma; LIHC, liver hepatocellular carcinoma; LUAD, lung adenocarcinoma; MESO, mesothelioma; OV, ovarian serous cystadenocarcinoma; PAAD, pancreatic adenocarcinoma; PCPG, pheochromocytoma and paraganglioma; PRAD, prostate adenocarcinoma; READ, rectum adenocarcinoma; SARC sarcoma; SKCM, skin cutaneous melanoma; STAD, stomach adenocarcinoma; THCA, thyroid carcinoma; THYM, thymoma; UCEC, uterine corpus endometrial carcinoma; UVM, uveal melanoma.

immune pathway and immune cell analysis.

Given that the range of 63 genes is still too large for researchers to practically examine, PPI analysis was employed to further screen the genes that play a key role in pan-cancer. Subsequently, 15 genes were selected with a binding coefficient of >0.7, and their correlations were analyzed in relation to the pan-cancer immune, matrix, RNA stem cell, and DNA stem cell scores. Among all these 15 genes, the one with the highest immune and matrix scores was BRCT repeats of breast cancer, type 1 (*BRIP1*), which was negatively correlated with the immune score of most tumors but positively correlated with the stem cell score. The protein encoded by this gene is a member of the RecQ DEAH helicase family and interacts with the BRCT repeats of breast cancer, type 1 (*BRCA1*). Previous studies have demonstrated that *BRCA1* is a tumor-suppressor gene, and its mutations are known to increase susceptibility to many cancers, including breast, ovarian, pancreatic, and prostate cancer (24,25). The results of the present bioinformatics analysis indicated that *BRCA1* is highly expressed in most tumors and may be related to tumor stem cells. Furthermore, survival analysis revealed that *BRCA1* was associated with the poor prognosis of most tumors, such as pancreatic adenocarcinoma and adrenocortical carcinoma. This provides a new direction for the study of NK cell-related genes in pan-cancer.

Finally, the prognostic ability of the 15 genes was analyzed in pan-cancer, with the most prominent genes being *ASPM* and *DEPDC1*, as they were found to play a significant role in the prognosis of 12 and 14 tumor types, respectively.

ASPM (spindle microtubule assembly factor) is a protein-coding gene, which is mainly involved in cell mitosis, cell cycle progression, and DNA damage repair (26,27). Initially, research on *ASPM* focused on its mutations with autosomal recessive primary microcephaly [MicroCephaly Primary Hereditary (MCPH)], with mutations in *ASPM* accounting for over 40% of MCPH cases (28,29). In a recent study, Razuvaeva *et al.* hypothesized that mutations in *ASPM* inhibit the growth of neural progenitor cells, thereby impeding neurogenesis and leading to MCPH, thus providing a possible explanation for why *ASPM* mutations are the most commonly mutated genes in MCPH (30). Moreover, *ASPM* is also closely associated with the occurrence and development of various cancers (31-35). A study indicates that *ASPM* promotes the proliferation, migration, invasion, and stemness of malignant tumors via the WNT/β-catenin

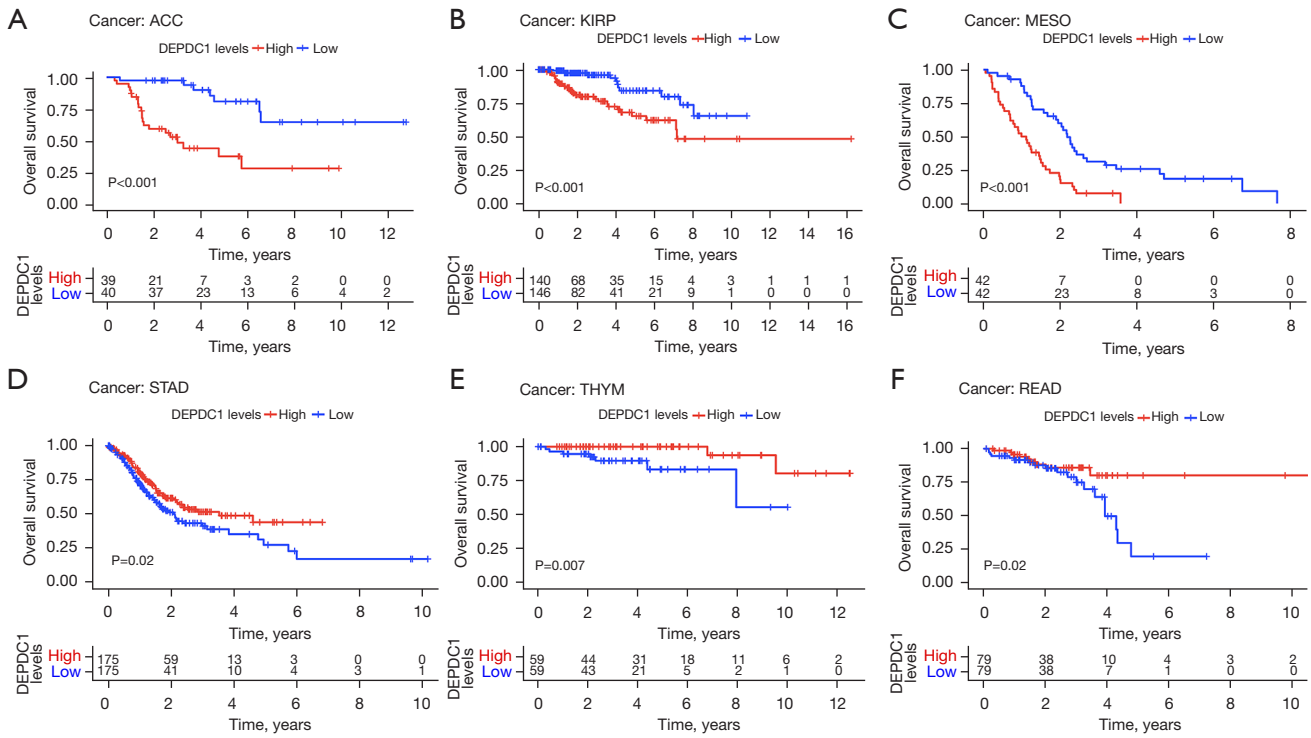

Figure 7 Kaplan-Meier survival curve of *DEPDC1* in six cancer types in the high and low gene expression groups. Low expression of *DEPDC1* is associated with better prognosis of ACC (A), KIRP (B), and MESO (C), while high expression of *DEPDC1* relates to better prognosis of STAD (D), THYM (E), and READ (F). ACC, adrenocortical carcinoma; KIRP, kidney renal papillary cell carcinoma; MESO, mesothelioma; STAD, stomach adenocarcinoma; THYM, thymoma; READ, rectum adenocarcinoma.

signaling pathway; for example, in the case of prostate cancer, *ASPM* maintains a subpopulation of prostate cancer stem cells by increasing the protein stability of disheveled-3 (Dvl-3), the cardinal upstream regulator of the canonical Wnt signaling pathway (36). Moreover, Tsai *et al.* suggest the clinical utility of *APSM* as a prognostic biomarker for cancer and propose viable molecular targeting and synthetic lethal approaches to leverage its therapeutic potential (27). The results of our bioinformatic analysis confirmed that *ASPM* is an oncogene that is upregulated in most tumors, and our study suggested, for the first time, that *ASPM* plays a significant role in the pan cancer immune microenvironment. Moreover, the possible associations of *ASPM* with THYM and uveal melanoma have not yet been reported. Further experiments should be conducted to confirm this result.

DEPDC1 is a DEP domain protein-coding gene containing 1, which is closely associated with poor prognosis in various malignant tumors, such as breast cancer, bladder cancer, osteosarcoma, and oral squamous cell carcinoma (37-40). Huang *et al.*, through the analysis of glycolysis-related genes, confirmed that *DEPDC1* promotes the malignant progression of oral squamous cell carcinoma through the WNT/β-catenin signaling pathway and suggest that DEPDC1 may be a novel biomarker and therapeutic target for oral squamous cell carcinoma (40). In our survival analysis, *DEPDC1* was associated with the poor prognosis of most tumors, including adrenocortical carcinoma, kidney renal clear cell carcinoma, kidney renal papillary cell carcinoma, and liver hepatocellular carcinoma (HCC), but interestingly, the presence of *DEPDC1* in COAD, STAD, and rectal adenocarcinoma was associated with a good prognosis. The good prognosis of STAD is consistent with another bioinformatics analysis study, in which a high level of *DEPDC1* expression was associated with a good progression-free interval in cases of STAD (41). However, another study revealed that a higher expression of *DEPDC1* was associated with poor prognosis in STAD, and further experimentation is needed to confirm whether the expression of *DEPDC1* is correlated with tumor metastasis

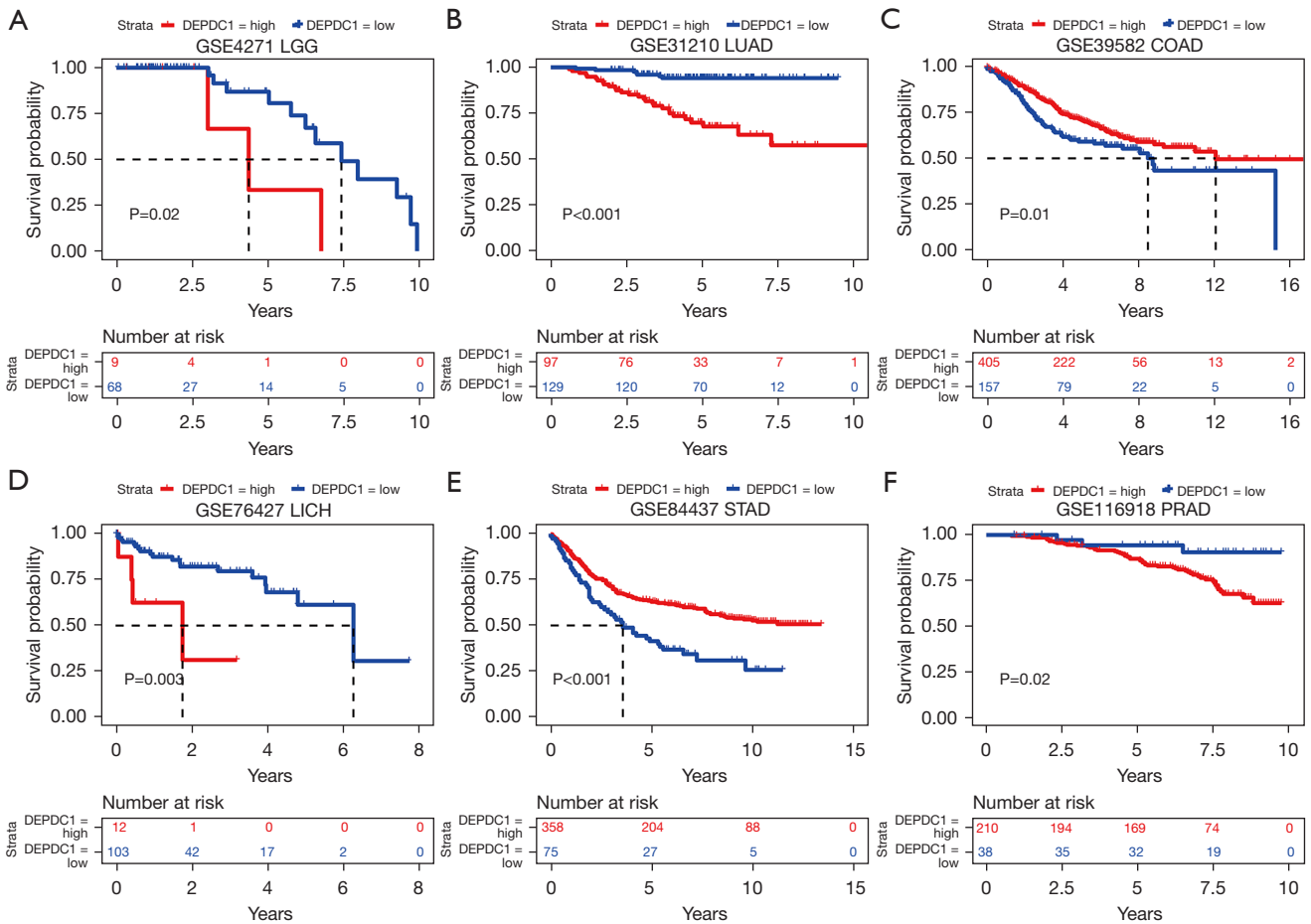

Figure 8 Pan-cancer prognostic survival curve of *DEPDC1*. The Kaplan-Meier survival curves show the differences in *DEPDC1* gene expression in the prognosis of pan-cancer. Better prognosis of COAD (C) and STAD (E) was associated with high *DEPDC1* gene expression, whereas low *DEPDC1* gene expression was associated with the better prognosis of LGG (A), LUAD (B), LICH (D), and PRAD (F). LGG, lower grade glioma; LUAD, lung adenocarcinoma; COAD, colon adenocarcinoma; LIHC, liver hepatocellular carcinoma; STAD, stomach adenocarcinoma; PRAD, prostate adenocarcinoma.

and differentiation (42). This inconsistency is likely due to differences in data processing and analytical tools; nevertheless, additional studies should be conducted to further clarify the relationship between *DEPDC1* expression and the prognosis of STAD.

As identified the most prominent NK cell-related genes in this research, both ASPM and DEPDC1 can promote the malignant progression of cancers through the WNT/β-catenin signaling pathway, which plays a significant role in various physiological processes such as cell proliferation, differentiation, migration (43). Increasing research has revealed the correlation between dysregulation of the Wnt/β-catenin signaling pathway and the development and progression of tumors, such as colorectal cancer, melanoma, and leukemia (44-46). Through a comprehensive literature review, a significant correlation was unveiled between NK cells and the WNT/β-catenin signaling pathway. Emerging evidence highlights the participation of the Wnt/β-catenin signaling pathway in the development and differentiation of NK cells (47,48). For instance, one study demonstrated that the introduction of DKK1, a natural inhibitor of β-catenin-dependent Wnt signal, results in diminished NK cell counts (49). Nevertheless, there exists some inconsistency regarding the impact of Wnt/β-catenin signaling pathway inhibition on NK cell activation and cytotoxicity. In one study, Xiao *et al.* proposed that the suppression of NK cell activation mediated by DKK2, also a natural inhibitor of Wnt signal, may be independent of the Wnt/β-catenin

signaling pathway (50). However, in gastrointestinal tumors, particularly HCC and gastric cancer (GC), ISG12a has been demonstrated to suppress Wnt/β-catenin signaling pathway, thereby downregulating PD-L1 expression and rendering cancer cells sensitive to NK cell-mediated death (51). Given the limited literature on the association between Wnt/β-catenin signaling and NK cells, this controversy deserves more attention and further exploration in the future.

Conclusions

This study investigated the role of NK cell-related genes in pan-cancer and constructed a prognostic model with 63 NK cell-related genes. Survival and ROC analyses employed prove the effectiveness of the model. In addition, the roles of the 63 NK cell-related genes in cancer were analyzed, and two significant genes were identified—*DEPDC1* and *ASPM*—that may offer a potential direction in tumor immune research.

We also further discovered that *DEPDC1* is variably related to the prognosis of 14 kinds of cancer; among these, the association between *DEPDC1* expression and the prognosis of STAD remains to be further explored. The association between *ASPM* expression and the poor prognosis of THYM and uveal melanoma has been characterized, which have not been examined in previous bioinformatics analyses. Although our research still has certain limitations, including missing clinical cohort data and a lack of experimental verification to evaluate the analysis results, our findings potentially open new avenues of research in this field.

Acknowledgments

Funding: None.

Footnote

Reporting Checklist: The authors have completed the TRIPOD reporting checklist. Available at https://tcr.amegroups.com/article/view/10.21037/tcr-24-434/rc

Peer Review File: Available at https://tcr.amegroups.com/article/view/10.21037/tcr-24-434/prf

Conflicts of Interest: All authors have completed the ICMJE uniform disclosure form (available at https://tcr.amegroups.com/article/view/10.21037/tcr-24-434/coif). The authors have no conflicts of interest to declare.

Ethical Statement: The authors are accountable for all aspects of the work in ensuring that questions related to the accuracy or integrity of any part of the work are appropriately investigated and resolved. Besides, the study was conducted in accordance with the Declaration of Helsinki (as revised in 2013).

References

1. Romee R, Foley B, Lenvik T, et al. NK cell CD16 surface expression and function is regulated by a disintegrin and metalloprotease-17 (ADAM17). Blood 2013;121:3599-608.
2. Yu J, Venstrom JM, Liu XR, et al. Breaking tolerance to self, circulating natural killer cells expressing inhibitory KIR for non-self HLA exhibit effector function after T cell-depleted allogeneic hematopoietic cell transplantation. Blood 2009;113:3875-84.
3. Khan M, Arooj S, Wang H. NK Cell-Based Immune Checkpoint Inhibition. Front Immunol 2020;11:167.
4. Xie G, Dong H, Liang Y, et al. CAR-NK cells: A promising cellular immunotherapy for cancer. EBioMedicine 2020;59:102975.
5. Marofi F, Saleh MM, Rahman HS, et al. CAR-engineered NK cells; a promising therapeutic option for treatment of hematological malignancies. Stem Cell Res Ther 2021;12:374.
6. Chen Z, Hu Y, Mei H. Advances in CAR-Engineered Immune Cell Generation: Engineering Approaches and Sourcing Strategies. Adv Sci (Weinh) 2023;10:e2303215.
7. Zhang H, Yang L, Wang T, et al. NK cell-based tumor immunotherapy. Bioact Mater 2023;31:63-86.
8. Kearney CJ, Vervoort SJ, Hogg SJ, et al. Tumor immune evasion arises through loss of TNF sensitivity. Sci Immunol 2018;3:eaar3451.
9. Freeman AJ, Vervoort SJ, Ramsbottom KM, et al. Natural Killer Cells Suppress T Cell-Associated Tumor Immune

Evasion. Cell Rep 2019;28:2784-2794.e5.
10. Sheffer M, Lowry E, Beelen N, et al. Genome-scale screens identify factors regulating tumor cell responses to natural killer cells. Nat Genet 2021;53:1196-206.
11. Vyas J, Gryk MR, Schiller MR. VENN, a tool for titrating sequence conservation onto protein structures. Nucleic Acids Res 2009;37:e124.
12. Smyth GK. limma: Linear Models for Microarray Data. In: Gentleman R, Carey VJ, Huber W, et al. editors. Bioinformatics and Computational Biology Solutions Using R and Bioconductor. Statistics for Biology and Health. New York, NY: Springer; 2005:397-420.
13. Kolde R, Laur S. RobustRankAggreg: Methods for robust rank aggregation. Bioinformatics 2012;28:573-80.
14. Hastie T, Tibshirani R, Tibshirani R. Best subset, forward stepwise or lasso? Analysis and recommendations based on extensive comparisons. Statist Sci 2020;35:579-92.
15. Therneau T. A package for survival analysis in S. R package version 2015;2.
16. Barbie DA, Tamayo P, Boehm JS, et al. Systematic RNA interference reveals that oncogenic KRAS-driven cancers require TBK1. Nature 2009;462:108-12.
17. Newman AM, Steen CB, Liu CL, et al. Determining cell type abundance and expression from bulk tissues with digital cytometry. Nat Biotechnol 2019;37:773-82.
18. von Mering C, Huynen M, Jaeggi D, et al. STRING: a database of predicted functional associations between proteins. Nucleic Acids Res 2003;31:258-61.
19. Chen B, Khodadoust MS, Liu CL, et al. Profiling Tumor Infiltrating Immune Cells with CIBERSORT. Methods Mol Biol 2018;1711:243-59.
20. Azad NS, Gray RJ, Overman MJ, et al. Nivolumab Is Effective in Mismatch Repair-Deficient Noncolorectal Cancers: Results From Arm Z1D-A Subprotocol of the NCI-MATCH (EAY131) Study. J Clin Oncol 2020;38:214-22.
21. Marigo I, Zilio S, Desantis G, et al. T Cell Cancer Therapy Requires CD40-CD40L Activation of Tumor Necrosis Factor and Inducible Nitric-Oxide-Synthase-Producing Dendritic Cells. Cancer Cell 2016;30:377-90.
22. Horowitz A, Strauss-Albee DM, Leipold M, et al. Genetic and environmental determinants of human NK cell diversity revealed by mass cytometry. Sci Transl Med 2013;5:208ra145.
23. Shechner DM, Hacisuleyman E, Younger ST, et al. Multiplexable, locus-specific targeting of long RNAs with CRISPR-Display. Nat Methods 2015;12:664-70.
24. Volcic M, Karl S, Baumann B, et al. NF-κB regulates DNA double-strand break repair in conjunction with BRCA1-CtIP complexes. Nucleic Acids Res 2012;40:181-95.
25. Gupta R, Liu AY, Glazer PM, et al. LKB1 preserves genome integrity by stimulating BRCA1 expression. Nucleic Acids Res 2015;43:259-71.
26. Jiang K, Rezabkova L, Hua S, et al. Microtubule minus-end regulation at spindle poles by an ASPM-katanin complex. Nat Cell Biol 2017;19:480-92.
27. Tsai KK, Bae BI, Hsu CC, et al. Oncogenic ASPM Is a Regulatory Hub of Developmental and Stemness Signaling in Cancers. Cancer Res 2023;83:2993-3000.
28. Kouprina N, Pavlicek A, Collins NK, et al. The microcephaly ASPM gene is expressed in proliferating tissues and encodes for a mitotic spindle protein. Hum Mol Genet 2005;14:2155-65.
29. Létard P, Drunat S, Vial Y, et al. Autosomal recessive primary microcephaly due to ASPM mutations: An update. Hum Mutat 2018;39:319-32.
30. Razuvaeva AV, Graziadio L, Palumbo V, et al. The Multiple Mitotic Roles of the ASPM Orthologous Proteins: Insight into the Etiology of ASPM-Dependent Microcephaly. Cells 2023;12:922.
31. Li N, Chu J, Hu K, et al. ASPM overexpression enhances cellular proliferation and migration and predicts worse prognosis for papillary renal cell carcinoma. J Biosci 2023;48:17.
32. Jiang L, Zhang S, An N, et al. ASPM Promotes the Progression of Anaplastic Thyroid Carcinomas by Regulating the Wnt/beta-Catenin Signaling Pathway. Int J Endocrinol 2022;2022:5316102.
33. Yuan YJ, Sun Y, Gao R, et al. Abnormal spindle-like microcephaly-associated protein (ASPM) contributes to the progression of Lung Squamous Cell Carcinoma (LSCC) by regulating CDK4. J Cancer 2020;11:5413-23.
34. Wang F, Li J, Liu J, et al. Controversial role of the possible oxyntic stem cell marker ASPM in gastric cancer. J Pathol 2017;241:559-61.
35. Chen X, Huang L, Yang Y, et al. ASPM promotes glioblastoma growth by regulating G1 restriction point progression and Wnt-β-catenin signaling. Aging (Albany NY) 2020;12:224-41.
36. Pai VC, Hsu CC, Chan TS, et al. ASPM promotes prostate cancer stemness and progression by augmenting Wnt-Dvl-3-β-catenin signaling. Oncogene 2019;38:1340-53. Erratum in: Oncogene 2019;38:1354.
37. Harada Y, Kanehira M, Fujisawa Y, et al. Cell-permeable peptide DEPDC1-ZNF224 interferes with transcriptional repression and oncogenicity in bladder cancer cells. Cancer

Res 2010;70:5829-39.
38. Kretschmer C, Sterner-Kock A, Siedentopf F, et al. Identification of early molecular markers for breast cancer. Mol Cancer 2011;10:15.
39. Shen L, Li H, Liu R, et al. DEPDC1 as a crucial factor in the progression of human osteosarcoma. Cancer Med 2023;12:5798-808.
40. Huang G, Chen S, Washio J, et al. Glycolysis-Related Gene Analyses Indicate That DEPDC1 Promotes the Malignant Progression of Oral Squamous Cell Carcinoma via the WNT/β-Catenin Signaling Pathway. Int J Mol Sci 2023;24:1992.
41. Jia B, Liu J, Hu X, et al. Pan-cancer analysis of DEPDC1 as a candidate prognostic biomarker and associated with immune infiltration. Ann Transl Med 2022;10:1355.
42. Gong Z, Chu H, Chen J, et al. DEPDC1 upregulation promotes cell proliferation and predicts poor prognosis in patients with gastric cancer. Cancer Biomark 2021;30:299-307.
43. Zhang Y, Wang X. Targeting the Wnt/β-catenin signaling pathway in cancer. J Hematol Oncol 2020;13:165.
44. Yuan S, Tao F, Zhang X, et al. Role of Wnt/β-Catenin Signaling in the Chemoresistance Modulation of Colorectal Cancer. Biomed Res Int 2020;2020:9390878.
45. Gajos-Michniewicz A, Czyz M. WNT Signaling in Melanoma. Int J Mol Sci 2020;21:4852.
46. Wang H, Qiu Y, Zhang H, et al. Histone acetylation by HBO1 (KAT7) activates Wnt/β-catenin signaling to promote leukemogenesis in B-cell acute lymphoblastic leukemia. Cell Death Dis 2023;14:498.
47. Bourayou E, Golub R. Signaling Pathways Tuning Innate Lymphoid Cell Response to Hepatocellular Carcinoma. Front Immunol 2022;13:846923.
48. Haseeb M, Pirzada RH, Ain QU, et al. Wnt Signaling in the Regulation of Immune Cell and Cancer Therapeutics. Cells 2019;8:1380.
49. Grzywacz B, Kataria N, Kataria N, et al. Natural killer-cell differentiation by myeloid progenitors. Blood 2011;117:3548-58.
50. Xiao Q, Wu J, Wang WJ, et al. DKK2 imparts tumor immunity evasion through β-catenin-independent suppression of cytotoxic immune-cell activation. Nat Med 2018;24:262-70.
51. Deng R, Zuo C, Li Y, et al. The innate immune effector ISG12a promotes cancer immunity by suppressing the canonical Wnt/β-catenin signaling pathway. Cell Mol Immunol 2020;17:1163-79.

Cite this article as: Li C, Huang Y, Yi X, Tang Y, Okita R, He J. Pan-cancer prognostic model and immune microenvironment analysis of natural killer cell-related genes. Transl Cancer Res 2024;13(4):1936-1953. doi: 10.21037/tcr-24-434

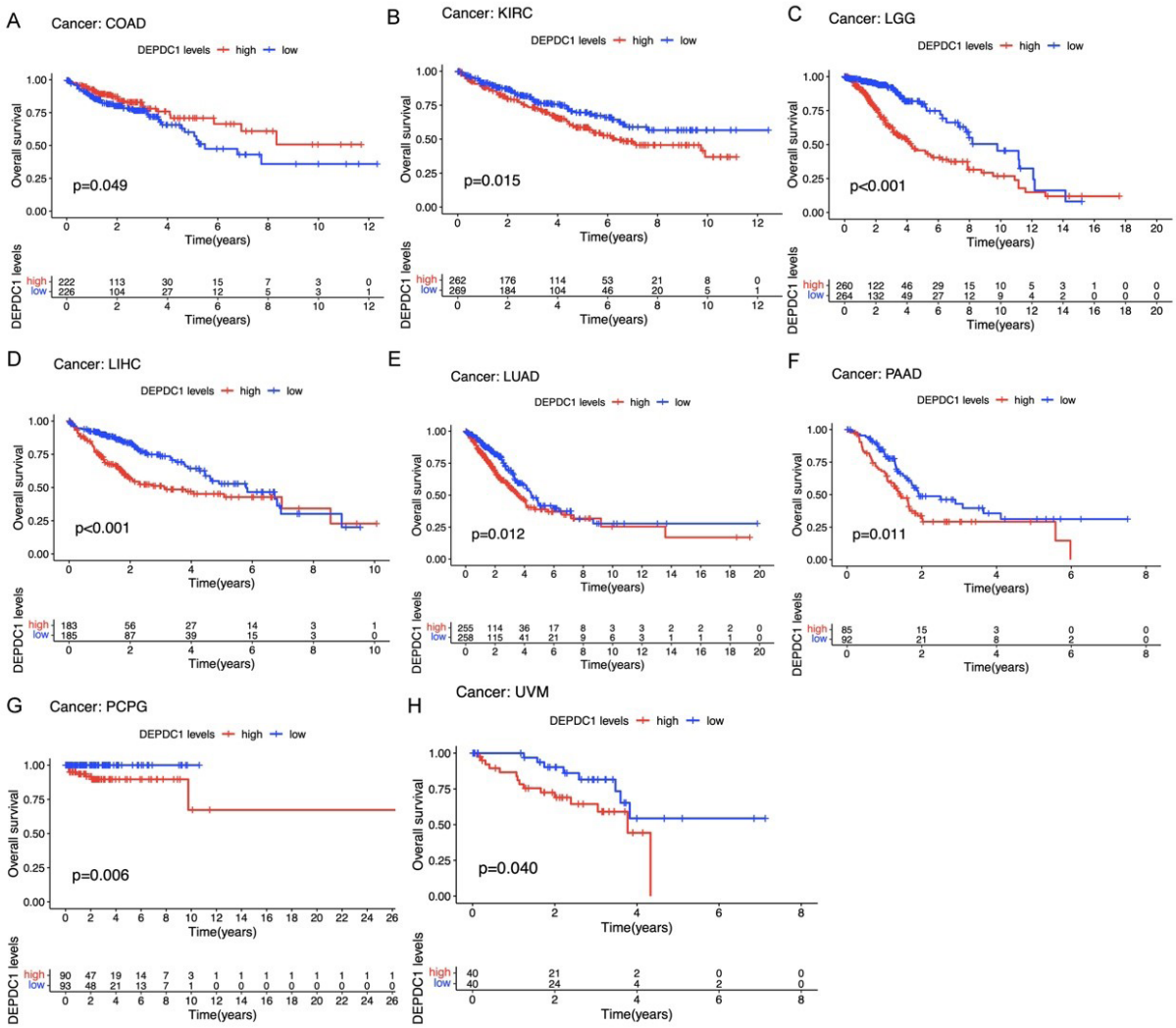

Figure S1 Kaplan-Meier survival curve of *DEPDC1* in the remaining 8 cancer types in the high and low gene expression groups. Low expression of *DEPDC1* is associated with better prognosis of KIRC (B), LGG (C), LIHC (D), LUAD (E), PAAD (F), PCPG (G), and UVM (H), while high expression of *DEPDC1* relates to better prognosis of COAD (A). COAD, colon adenocarcinoma; KIRC, kidney renal clear cell carcinoma; LGG, lower grade glioma; LIHC, liver hepatocellular carcinoma; LUAD, lung adenocarcinoma; PAAD, pancreatic adenocarcinoma; PCPG, pheochromocytoma and paraganglioma; UVM, uveal melanoma.

https://dx.doi.org/10.21037/tcr-24-434

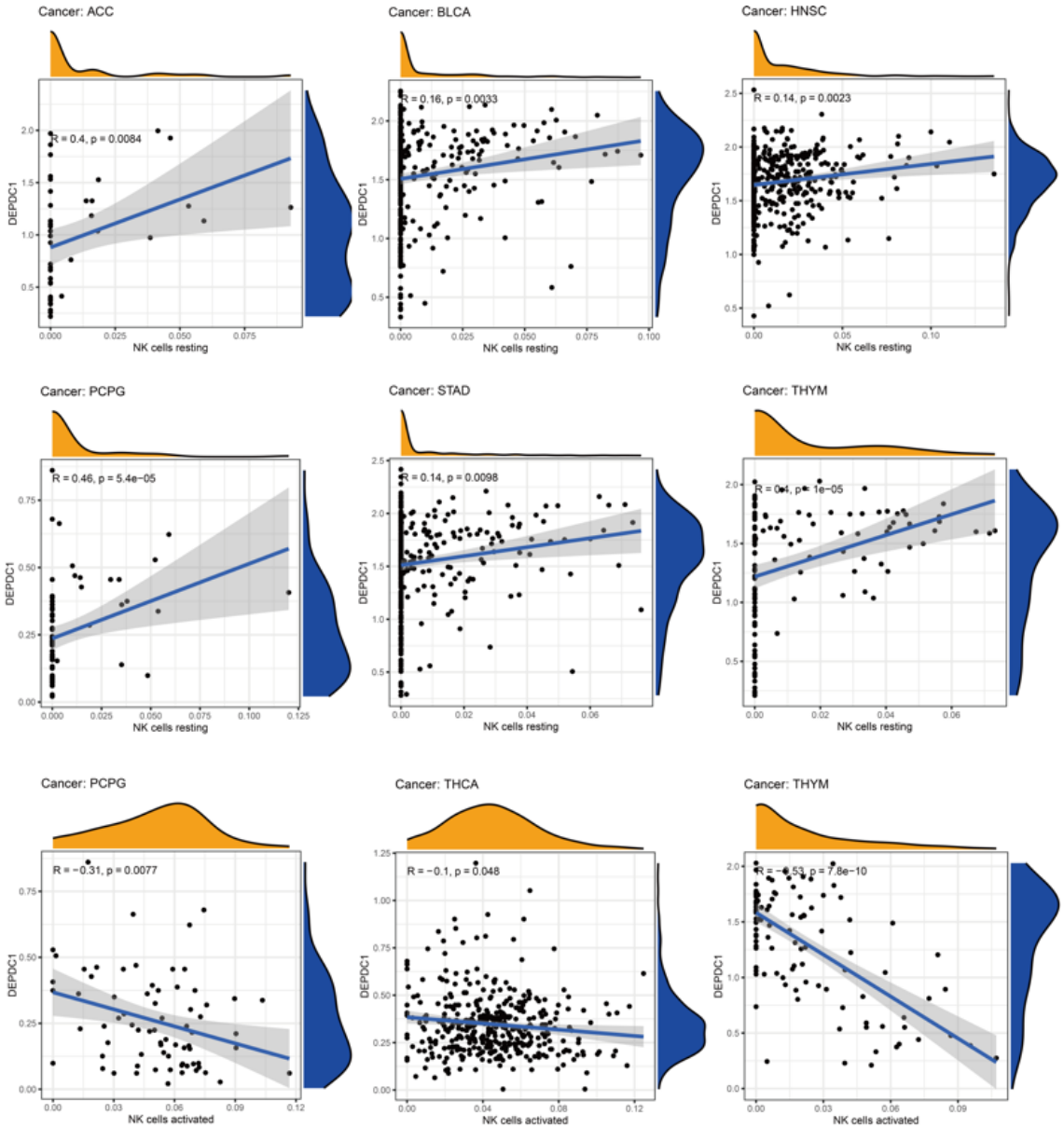

Figure S2 *DEPDC1* expression was positively correlated with resting NK cells in ACC, BLCA, HNSC, PCPG, STAD, and THYM. Interestingly, *DEPDC1* expression was negatively correlated with activated NK cells in PCPG, THCA and THYM. NK, natural killer; ACC, adrenocortical carcinoma; BLCA, bladder urothelial carcinoma; HNSC, head and neck squamous cell carcinoma; PCPG, pheochromocytoma and paraganglioma; STAD, stomach adenocarcinoma; THYM, thymoma; THCA, thyroid carcinoma.

https://dx.doi.org/10.21037/tcr-24-434

Table S1 Multivariate Cox analysis of natural killer cell-related genes in pan-cancer

ID	Coefficient
CYB5A	0.209203287
HERC1	–0.396818077
DNAJB6	–0.340244609
EFEMP1	0.209407629
UGP2	–0.359692172
SRXN1	0.253445713
MICAL3	–0.233035428
DAZAP2	0.353593961
CFAP69	–0.296107818
CRY2	–0.208398857
ARHGAP24	0.10500651
RNF31	0.262679557
AKAP12	0.23523783
DMGDH	–0.183691249
SHC2	0.087176503
PLIN2	0.101709133
LRRC27	–0.283934214
UACA	–0.346231223
MZF1	0.398820091
CCAR2	–0.754938219
C1QTNF1	0.122918785
SOX10	–34.81540786
KANK3	–0.259718166
ANXA6	–0.37529682
ME3	0.139756866
HFM1	–0.243793369
PITPNM2	0.135243256
CMYA5	0.109237695
SPTBN1	0.373898319
WDR20	–0.347167709
VEGFA	0.201191226
THBS3	0.558634422
TREM2	0.144696276
MET	0.165459283
SPINT1	–0.100316545
POLE3	–0.631989365
ASPM	0.438343033
MRPL15	0.423614623
E2F8	0.18179801
DEPDC1	0.232650878
BRIP1	–0.337048763
TAP1	–0.233396806
B4GALT5	0.505479247
TMEM81	0.240815354
PYGO2	–0.484521811
PRR15L	–0.151076764
MSANTD3	0.499313395
SLC35C1	0.481824306
STK4	0.334719638
IKZF3	–0.220809824
RELB	–0.171546659
SLC35B3	–0.358382922
POLR1B	–0.457944621
NRBF2	0.362408212
PFKFB4	–0.128519561
PDP1	–0.365689352
OXTR	0.087985839
ZIC2	0.107961896
ITPKC	0.193191373
HSPA4	0.365339059
BCAN	0.179748154
RAC1	0.881184261
SCAMP5	–0.106155254

https://dx.doi.org/10.21037/tcr-24-434